Comparisons and scaling rules between $N+N_2$ and N_2+N_2 collision induced dissociation cross sections from atomistic studies

F Esposito[1], E Garcia[2], and A Laganà[3]

[1] Consiglio Nazionale delle Ricerche, Nanotec, PLASMI Lab, Via Amendola 122/d, Bari (Italy)

[2] Departamento de Quimica Fisica, Universidad del Pais Vasco (UPV/EHU), Paseo de la Universidad 7, Vitoria (Spain)

[3] Dipartimento di Chimica, Biologia e Biotecnologie, Università degli studi di Perugia, Via Elce di Sotto 8, Perugia (Italy)

E-mail: fabrizio.esposito@cnr.it,e.garcia@ehu.es,lagana05@gmail.com

Abstract.

Quantitative knowledge of elementary processes involved in plasmas are key to successfully perform accurate kinetic simulations. The issue is the huge amount of data to treat, both in the dynamical calculation and in the kinetic simulation. The aim of this paper is to study the dissociation in atom-molecule and molecule-molecule collisions involving nitrogen, obtained by molecular dynamics considering vibrational states in the range 10-50 and collision energy up to 10 eV, in order to formulate suitable scaling laws resulting in less expensive computational procedures and easier to handle treatments in kinetic simulations. It is shown that, while a direct substitution of molecule-molecule dissociation cross sections with atom-molecule ones might be acceptable only at very high collision energy, scaling laws application allows to obtain quite good results on almost the whole energy range of interest.

Keywords: Nitrogen plasmas, Collision induced dissociation, Rate coefficients, Cross sections, Scaling rules

1. Introduction

Detailed information on the dynamics and kinetics of both Atom-Molecule (AM) and Molecule-Molecule (MM) collisions are of key importance in accurate modeling of aerothermodynamics, combustion, laser and plasma physics [1–19]. Complete sets of efficiency parameters are needed, under the form of thermal Rate Coefficients (RC) for single and multi-quantum vibrational energy transfers and Collision Induced Dissociation (CID) processes. High level RC computational procedures are usually articulated as follows: (1) building a suitably accurate Potential Energy Surface (PES) describing the interaction between the colliding atoms and molecules; (2) running on

the built PES extended molecular dynamics calculations (typically large batches of quasiclassical trajectories) whose initial conditions are chosen in order to match the conditions of interest.

As to step (1), in the past a large number of studies have been performed to the end of formulating full-dimensional PESs for N+N_2 and N_2+N_2, two collisional systems of particular importance. In 1987 a London-Eyring-Polanyi-Sato (LEPS) PES was proposed by some of us for N+N_2 [20]. This LEPS is a semi-empirical collinearly dominant PES that exhibits a smooth monotonic approach to the strong interaction region. This empirical PES was further improved using the largest-angle rotating bond-order (LAGROBO) methodology to fit a set of available high-level ab initio data describing the minimum energy path of the process and its dependence on the collision angle [21, 22]. The resulting Minimum Energy Path (MEP) exhibits a double barrier structure with a shallow well sandwiched between an early and a late barrier. Further ab initio calculations were performed later and two new full-dimensional surfaces were published [23, 24], both confirming a double barrier structure for the N+N_2 MEP.

For N_2+N_2 the investigation has focused initially only on the inelastic channel. Accordingly, the PES was initially formulated as a sum of the two N_2 intramolecular interactions and of an intermolecular component (ie that of two separated nitrogen molecules with their internuclear distances close to equilibrium) described in terms of isotropic and anisotropic contributions expanded in spherical harmonics (see for example refs [25–30]). That was later expressed in terms of a bond-bond pairwise additive interaction [31]. In order to overcome the bias of such formulation of the PES preventing a proper treatment of atom exchange processes and of the fragmentation of one (or both) molecule(s), extensive ab initio studies were performed for a wide set of molecular geometries and related outcomes were used for obtaining a full-dimensional more rigorous description of the interaction governing the N_2+N_2 collisions. A first work along this direction was reported in ref [32]. A more complete effort to deal with the problem of describing the N_2+N_2 reactive processes was made by the authors of ref [33], by carrying out ab initio computations for 16435 geometries describing nine N_2+N_2 and three N+N_3 arrangements. Then, this set of potential energy values was fitted both to a polynomial of bond-order variables [33, 34] and to a statistically localized, permutationally invariant, local moving least squares interpolating function [35]. The same set of data was used to build a PES as a sum of bond, valence angle, torsion angle, van der Waals and Coulombic energy interaction terms among all atom pairs [36]. More recently, based on the same set of ab initio values, a new polynomial function was proposed including a Gaussian contribution in the definition of the bond-order variables [37]. This feature enables that PES to validly describe high energy processes (including dissociation) and consistently formulates two, three and four body components (e.g. it reproduces the double barrier structure of the triatomic N+N_2 subsystem when one nitrogen atom is displaced to very large distances).

As to step (2), various dynamical and kinetics calculations for both N+N_2 and N_2+N_2 systems have been performed. In particular, calculations for reaction and energy

transfer in the N+N_2 collisions have been reported, for instance, in refs [21, 22, 38–51] and calculations for inelastic energy transfer as well as for reactive and dissociative processes in N_2+N_2 collisions have been reported in refs [52–56] and refs [5, 37, 57–61], respectively. However, there is a lack of comprehensive studies due mainly, as will be commented in more detail later, to the large number of trajectories to be integrated in order to work out with sufficient accuracy the relevant RC values. Moreover, when modeling the above mentioned environments, the production of complete sets of RCs for single and multi-quantum vibrational energy transfers and dissociation processes is just the initial step for some complex kinetic/fluidynamic codes which are themselves extremely computationally expensive and may require to explore a wide range of different microscopic conditions of the involved molecular systems.

For this reason, in the paper we tackle the problem of working out relationships among the needed efficiency parameters (starting from the CID RCs of both N+N_2 and N_2+N_2 processes) with the goal of finding out how to reduce the heavy associated computational work. Accordingly the paper is articulated as follows: in section 2 measured and computed AM and MM thermal RCs are compared in order to figure out their distinctive features and possible relationships between them; in section 3 the detailed components of the CID RCs are analyzed in order to learn for some of their subsets how one can use for that purpose more atomistic quantities like the Cross Sections (CSs); in section 4 the different articulations of the theoretical and computational methods used for computing CID thermal RCs and detailed CSs are illustrated; in section 5 a state-specific analysis of the computed AM and MM CID CSs is performed in order to characterize the distinctive atomistic features of the investigated processes and how they ground possible model relationships; in section 6 and 7 some key features of vibrationally cold-excited and excited-excited subsets of MM CID collisions are discussed and the same is done for some state-specific AM and MM CID CSs to the end of building highly efficient and inexpensive procedures for simplified calculations; in section 8 final conclusions and possible follow-ups are presented.

2. Experimental versus theoretical values of the N+N_2 and N_2+N_2 CID RCs

In order to get inspiration on how to proceed to trace back the MM RC values to the AM ones, we took advantage of the fact that, as already mentioned, the PES of ref [37] can be consistently used for evaluating both diatom-diatom and atom-diatom CID RCs and that the related experimental data are available. The most recent experimental sets of data for the CID RCs of molecular nitrogen by N_2 (solid red line) and N (solid black line) [62] are shown in fig 1 including those obtained by extrapolation (dashed segments). Experimental data were obtained by time-resolved optical interferometry from a free-piston shock tube without inert gas dilution, for temperatures ranging from 6,000 to 14,000 K. As apparent from the figure, the CID RCs of both N+N_2 and N_2+N_2 processes show a significant increase with the temperature (about four orders of

magnitude). Very important for the purpose of the present work is the fact that, in the whole range of temperature, dissociation of molecular nitrogen by the atom is always more effective than that from the molecule (by a factor of two at $T = 6,000$ K and a factor of five at $T = 14,000$ K). This trend agrees also with the findings of previous experimental measurements [63–65] not reported here for the sake of clarity. In fig 1 we plot for comparison also the theoretical estimates of the AM and MM CID thermal RCs (respectively black and red squares) obtained by us by running quasiclassical trajectories on the PES of ref [37] for the temperature interval ranging from $6,000$ to $30,000$ K (the method used to calculate the thermal RCs is given later in eq 6). Contrary to the experimental findings, the computed MM thermal RCs (thermalized at the same temperature for translational, vibrational and rotational degrees of freedom as specified in section 4) appear to only slightly differ from AM RCs. The calculated AM and MM RCs agree with the experimental AM data at about $T = 13,000$ K and $T = 7,000$ K, respectively. Outside this interval the computed values (especially the extrapolated ones) are larger than the experimental data.

The conflicting (computation versus experiment) indications about the possibility of a straightforward replacement of MM CID RCs by the AM ones provided by fig 1, prompted a more careful investigation of the atomistic ground for such difference. In particular, the fact that at both ends of temperature interval computed RCs are larger and miss the gap between measured AM and MM values casts doubts about the adequacy of assuming thermal equilibrium when computing RCs in systems in strong disequilibrium. After all, this aspect has been already discussed in the literature (see for example refs [66, 67]). For this reason in the remainder of the paper we shall deal with state-specific CS values (rather than the thermal RC ones) and try to develop detailed CS [68] scaling laws despite their intrinsic heavier computational cost. We shall focus on the dependence of CID CSs on the initial vibration in AM and MM collisions, an effect that is often smoothed by thermalization. For the purpose of calculating these quantities, we have leveraged on the presently available advanced networked computing capabilities of the European Grid Initiative (EGI) [69] and on the highly collaborative scheme of GEMS (Grid Empowered Molecular Simulator) [70–72] whose workflow masters the distributed execution of the various modules of the computation of the detailed AM and MM CID CSs.

3. The involved detailed quantities

As just mentioned, in this work we illustrate and analyze the computed AM and MM CID CSs of a nitrogen molecule colliding either with a nitrogen atom or another nitrogen molecule.

The AM collisions, $N^{(1)}$–$N^{(2)}(v_1, j_1)$ + $N^{(3)}$, can lead to the following four channels:

$$\begin{array}{lll} \mathrm{N^{(1)}}\text{–}\mathrm{N^{(2)}}(v_1', j_1') + \mathrm{N^{(3)}} & \mathrm{n} & (\mathrm{AM1}) \\ \mathrm{N^{(1)}}\text{–}\mathrm{N^{(3)}}(v', j') + \mathrm{N^{(2)}} & \mathrm{r} & (\mathrm{AM2}) \\ \mathrm{N^{(2)}}\text{–}\mathrm{N^{(3)}}(v', j') + \mathrm{N^{(1)}} & \mathrm{r} & (\mathrm{AM3}) \\ \mathrm{N^{(1)}} + \mathrm{N^{(2)}} + \mathrm{N^{(3)}} & \mathrm{d} & (\mathrm{AM4}) \end{array}$$

where v and j are the vibrational and rotational quantum numbers, respectively, and unprimed quantities refer to the initial arrangement while primed quantities refer to the final one. Note that atoms are labeled in order to make them distinguishable. Moreover, channels are classified as: non-reactive (n) when the original arrangement is retained while vibrational and rotational quantum numbers as well as translational energy may vary; reactive (r) when the colliding atom replaces one of the atoms of the molecule and translational energy and vibrational and rotational quantum numbers as well may vary; and dissociative (d) when the molecule dissociates and all three atoms fly apart separately.

Accordingly, the above mentioned channel AM1 is non-reactive, channels AM2 and AM3 are reactive and channel AM4 is dissociative with the CID RC being defined as:

$$-\frac{\mathrm{d}[\mathrm{N_2}]}{\mathrm{d}t} = \frac{1}{2}\frac{\mathrm{d}[\mathrm{N}]}{\mathrm{d}t} = k_{\mathrm{AM4}}\,[\mathrm{N_2}]\,[\mathrm{N}] = k_{\mathrm{AM}}\,[\mathrm{N_2}]\,[\mathrm{N}] \tag{1}$$

where k_{AM} denotes the dissociation RC for the AM processes.

The MM collisions, $\mathrm{N^{(1)}}$–$\mathrm{N^{(2)}}(v_1, j_1) + \mathrm{N^{(3)}}$–$\mathrm{N^{(4)}}(v_2, j_2)$, can lead to the following ten channels:

$$\begin{array}{lll} \mathrm{N^{(1)}}\text{–}\mathrm{N^{(2)}}(v_1', j_1') + \mathrm{N^{(3)}}\text{–}\mathrm{N^{(4)}}(v_2', j_2') & \mathrm{n} & (\mathrm{MM1}) \\ \mathrm{N^{(1)}}\text{–}\mathrm{N^{(3)}}(v', j') + \mathrm{N^{(2)}}\text{–}\mathrm{N^{(4)}}(v'', j'') & \mathrm{r} & (\mathrm{MM2}) \\ \mathrm{N^{(1)}}\text{–}\mathrm{N^{(4)}}(v', j') + \mathrm{N^{(2)}}\text{–}\mathrm{N^{(3)}}(v'', j'') & \mathrm{r} & (\mathrm{MM3}) \\ \mathrm{N^{(1)}}\text{–}\mathrm{N^{(2)}}(v_1', j_1') + \mathrm{N^{(3)}} + \mathrm{N^{(4)}} & \mathrm{nd} & (\mathrm{MM4}) \\ \mathrm{N^{(1)}}\text{–}\mathrm{N^{(3)}}(v', j') + \mathrm{N^{(2)}} + \mathrm{N^{(4)}} & \mathrm{rd} & (\mathrm{MM5}) \\ \mathrm{N^{(1)}}\text{–}\mathrm{N^{(4)}}(v', j') + \mathrm{N^{(2)}} + \mathrm{N^{(3)}} & \mathrm{rd} & (\mathrm{MM6}) \\ \mathrm{N^{(2)}}\text{–}\mathrm{N^{(3)}}(v', j') + \mathrm{N^{(1)}} + \mathrm{N^{(4)}} & \mathrm{rd} & (\mathrm{MM7}) \\ \mathrm{N^{(2)}}\text{–}\mathrm{N^{(4)}}(v', j') + \mathrm{N^{(1)}} + \mathrm{N^{(3)}} & \mathrm{rd} & (\mathrm{MM8}) \\ \mathrm{N^{(3)}}\text{–}\mathrm{N^{(4)}}(v_2', j_2') + \mathrm{N^{(1)}} + \mathrm{N^{(2)}} & \mathrm{nd} & (\mathrm{MM9}) \\ \mathrm{N^{(1)}} + \mathrm{N^{(2)}} + \mathrm{N^{(3)}} + \mathrm{N^{(4)}} & \mathrm{d} & (\mathrm{MM10}) \end{array}$$

where the channels are classified as: reactive events (r) when two new (diatomic) molecules are formed with an atom being replaced by one of those of the other initial molecule and full dissociative events (d) when both molecules dissociate and four separated atoms are formed. In MM collisions two new kinds of processes take place: non-reactive dissociative processes (nd) when only one reactant molecule dissociates leading to two separated atoms while the other reactant molecule retains its identity though its internal energy may vary; and reactive dissociative processes (rd) when one molecule is formed with one atom from each of the reactants with the other two atoms flying apart separately. There are four rd processes (namely, MM5, MM6, MM7, and MM8), two nd processes (MM4, MM9) and two r processes (MM2, MM3). In this case,

the CID RC is defined by:

$$-\frac{\mathrm{d}[\mathrm{N_2}]}{\mathrm{d}t} = \frac{1}{2}\frac{\mathrm{d}[\mathrm{N}]}{\mathrm{d}t} = k_{\mathrm{MM4}}\,[\mathrm{N_2}]^2 + k_{\mathrm{MM5}}\,[\mathrm{N_2}]^2 + k_{\mathrm{MM6}}\,[\mathrm{N_2}]^2 + k_{\mathrm{MM7}}\,[\mathrm{N_2}]^2 + k_{\mathrm{MM8}}\,[\mathrm{N_2}]^2 + k_{\mathrm{MM9}}\,[\mathrm{N_2}]^2 + 2\,k_{\mathrm{MM10}}\,[\mathrm{N_2}]^2 = k_{\mathrm{nd}}\,[\mathrm{N_2}]^2 + k_{\mathrm{rd}}\,[\mathrm{N_2}]^2 + 2\,k_{\mathrm{d}}\,[\mathrm{N_2}]^2 = k_{\mathrm{MM}}\,[\mathrm{N_2}]^2 \quad (2)$$

where $k_{\mathrm{nd}} = k_{\mathrm{MM4}} + k_{\mathrm{MM9}}$, $k_{\mathrm{rd}} = k_{\mathrm{MM5}} + k_{\mathrm{MM6}} + k_{\mathrm{MM7}} + k_{\mathrm{MM8}}$, $k_{\mathrm{d}} = k_{\mathrm{MM10}}$ and the overall dissociation RC for the MM processes is $k_{\mathrm{MM}} = k_{\mathrm{nd}} + k_{\mathrm{rd}} + 2\,k_{\mathrm{d}}$.

In the present paper we adopted, as already mentioned, an atomistic approach in which processes are analyzed in terms of CID cross sections (σ) which are quantities depending on the collision energy E and individual internal states v and j for vibration and rotation, respectively. Accordingly, as from eqs 1 and 2, the quantities considered for the AM and MM processes are defined as:

$$\sigma_{\mathrm{AM}} = \sigma_{\mathrm{AM4}} \quad (3)$$

$$\sigma_{\mathrm{MM}} = \sigma_{\mathrm{nd}} + \sigma_{\mathrm{rd}} + 2\,\sigma_{\mathrm{d}} = \sigma_{\mathrm{MM4}} + \sigma_{\mathrm{MM5}} + \sigma_{\mathrm{MM6}} + \sigma_{\mathrm{MM7}} + \sigma_{\mathrm{MM8}} + \sigma_{\mathrm{MM9}} + 2\,\sigma_{\mathrm{MM10}} \quad (4)$$

4. Theoretical methodology for computing state-specific CID CSs

Dissociation cross sections were computed using the Quasi-Classical Trajectory (QCT) method as implemented in the program VENUS96 [73]. The QCT method assumes that the nuclei involved in a bimolecular collision move according to the laws of classical mechanics on the potential energy surface of the system. By integrating the relative Hamilton equations the coordinates and momenta of all nuclei are calculated at every time step during the collision. Initial values of the coordinates and momenta are determined by setting the internal energy states of the molecules to correspond to quantum states. The integration is carried out until the fragments produced by the collision are sufficiently separated. Then, the species produced are identified and the channel is assigned. The result of the integration is a set of final values for coordinates and momenta of all nuclei. Using such information, final properties of the system are evaluated, for instance the internal energies and rotational angular momenta of the molecules, the (approximate and continuous) rotational (rqn) and vibrational (vqn) 'quantum numbers' of molecules worked out semi-classically [74], the relative translational energy, the scattering angle, etc. For both the AM and MM calculations use was made of the already mentioned most recent PES [37].

In order to estimate the dynamical properties of the investigated systems, a statistically significant sample of trajectories has been integrated and related outcomes averaged. To this end, a Monte Carlo procedure requires a large set of trajectories randomly selected in the spatial orientation of the molecules, the phase of the vibrational motion and the spatial orientation of the diatom's internal angular momentum vector.

In the QCT framework, for channel i the cross section at the collision energy E is given by the relationship:

$$\sigma_i(E) = \pi\, b_{\max}^2\, \frac{N_i}{N} \tag{5}$$

where N is the total number of trajectories integrated, N_i is the number of trajectories ending in channel i and $b_{\max}$ is the maximum value of the impact parameter for which channel i can be populated. The associated relative error is approximately proportional to $N_i^{-1/2}$.

The dynamical quantities considered in this paper are the already mentioned AM and MM CID CSs computed at a given initial value of the collision energy and at a given set of rovibrational states of the involved molecules. The investigated range of initial collision energy values varies from threshold to 10 eV, in steps of 0.1 eV. The considered initial vibrational states of the colliding molecules are 10, 20, 30, 40 and 50. The considered initial rotational states are 0, 40 and 80 (for the vibrational state of 50 the maximum rotational state considered was 40). Further details on the parameters used for the QCT calculations are: the integration step is 0.1 fs in order to guarantee a very good total energy and total angular momentum conservation; the initial and final distances between the collisional fragments to start and to end the trajectory integration are 14 Å in order to guarantee a negligible interaction between the fragments of the various channels; the impact parameter is chosen randomly in the interval $0 - b_{\max}$; the maximum impact parameter selected for both atom-molecule and molecule-molecule calculations is 9 Å, in order to ensure that all dissociative collisions are taken into account. In all cases, the number of integrated trajectories for a given collision energy and a given rovibrational state of the molecule is $N = 1 \times 10^5$ in order to lead to an error of the dissociation cross section smaller than 1%.

In the most general case, thermal RC for a given channel i is computed from the corresponding CS averaging over both the collision energy and the population of the initial rovibrational states:

$$k_i(T) = \sum_{v_1}\sum_{j_1} \frac{g_{j_1}\, e^{E_{\rm int}(v_1,j_1)/k_{\rm B}T}}{\sum_{v_1}\sum_{j_1} g_{j_1}\, e^{E_{\rm int}(v_1,j_1)/k_{\rm B}T}} \left(\frac{8}{\pi\mu k_{\rm B}^3 T^3}\right)^{1/2} \int_0^\infty E\, \sigma_i(E, v_1, j_1) e^{-E/k_{\rm B}T} {\rm d}E \tag{6}$$

where $k_{\rm B}$ and μ are the Boltzmann's constant and the reduced mass of the colliding bodies, respectively, while g_{j_1} is the rotational degeneracy and $E_{\rm int}(v_1, j_1)$ is the internal energy of the rovibrational state (v_1, j_1). Note that this equation is valid to compute the thermal rate coefficient for the atom-molecule collisions, being that for molecule-molecule processes analogous. In the QCT framework, eq 6 can be reduced to the relationship [74]:

$$k_i(T) = \left(\frac{8}{\pi\mu k_{\rm B}^3 T^3}\right)^{1/2} \pi\, b_{\max}^2\, \frac{N_i}{N} \tag{7}$$

once both the collision energy and the initial rovibrational states supported by the diatomic potential curve are sampled according to the equilibrium thermal Boltzmann distribution at a temperature T. (Sometimes the assumption of a temperature common to all the degrees of freedom is mitigated by restraining it only to some of them, like in the case of the two- and three-temperature kinetic models). Direct QCT calculation of RC by eq 7 is computationally much cheaper than by eq 6, due to the different weights implicitly attributed in eq 7 to the various states and collision energies.

For the MM calculations, a total of $N = 20 \times 10^6$ trajectories were integrated at $T = 30,000$ K, leading to an error on the CID RC lower than 0.1%. Yet N had to be increased to 600×10^6 at $T = 6,000$ K in order to obtain an error lower than 10%. In the case of AM calculations, the number of integrated trajectories varied from 5×10^6 to 400×10^6 in going from $T = 30,000$ K to $T = 6,000$ K in order to obtain errors similar to those of the MM calculations.

5. AM vs MM cross sections: on the trail for a model

In fig 2 the calculated values of the CID CSs are plotted as a function of the collision energy for MM using different symbols for the different initial v_2 values. For AM black lines are used. In all panels the same initial vibrational state v_1 is given to the molecule in AM collisions and to the hotter molecule in MM collisions. The value of v_1 increases across the panels from 20 to 50 in steps of 10. The MM colder molecule initial vibrational state v_2 ranges from 0 to v_1 in steps of 10 inside each panel (due to the symmetry of the collisional system, it is appropriate to restrict v_2 to values lower than or equal to v_1). The rotational energy of the initial molecules is set equal to zero unless differently specified.

The first annotation on the MM results shown in the figure is about their general shape that, as typical of processes with an activation energy, has an energy threshold followed by a first region of steady increase that gradually turns into a plateau at larger energies. In the figure this shape is completely shown only by the highest v_1 results, while for the lower ones the plateau is not reached.

Results are, however, extended enough to single out the marked sensitivity of cross sections to the vibrational excitation of the colder molecule, at a fixed v_1 value. To stress this point we found it useful to consider also the ratio MM(v_1, v_2)/MMo(v_1) where MMo$(v_1)\equiv$MM$(v_1, v_2 = 0)$, shown in fig 3. This ratio decreases rapidly after dissociation threshold till a steady value is reached. This steady value is about 1 for $v_2 = 10$ when $v_1 \geq 30$, but it can be larger for higher v_2 values. However, the higher v_1, the lower the MM(v_1, v_2)/MMo(v_1) ratio for any v_2 value at any given collision energy. This confirms the decreasing sensitivity of the MM CSs to v_2 variations for increasing v_1 values.

The second annotation on MM results shown in fig 2 is about the clear similarity between the AM(v_1) curve and the CS MM(v_1,v_2) ones. As a matter of fact, as already pointed out before, the curves of the detailed MM(v_1, v_2) results envelop the AM(v_1)

ones. Yet, the plots do not exhibit a unique correspondence between the AM curve and any specific MM v_2 initial vibrational state. The AM CS is, in fact, close to the CS MM(20,10) when $v_1 = 20$, but it lies between CS MM(30,20) and CS MM(30,10) when $v_1 = 30$, and between CS MM(40,20) and CS MM(40,10) when $v_1 = 40$. At the same time, when $v_1 = 50$ the AM CS is smaller than any other curve.

In order to help with the rationalization of the results, we plot the MM/AM cross section ratio in fig 4 where, once excluded the threshold region (where quasiclassical calculations are less accurate), a clear convergence of the MM and AM results becomes apparent and prompts the formulation of a proper scaling factor in order to model the effect of varying v_2 in MM collisions (an effect obviously missing in AM CSs but to be taken into account when using them to simulate the diatom-diatom case). The straightforward substitution of MM CSs with AM values, previously suggested for the relative thermal RC calculations, appears here to be acceptable only at high collision energy and after a correction by a constant scaling factor. Yet, it is not acceptable at all for the extreme case $v_2 \approx 0$ and $v_2 \approx v_1$, for which an AM/MM replacement would introduce a quite large variable error. In the $v_2 \approx v_1$ case (see fig 4), one might adopt a scaling factor of two (corresponding to the mean ratio between MM($v_1, v_2 = v_1$) and AM($v = v_1$) CSs), although only for collision energies quite away from the threshold value.

In order to develop a more elaborated model we plot in fig 5 the partitioning of the MM CSs into contributions depending on the final vqn of the non dissociating molecule. In this figure, v_1 is equal to 30 while v_2 increases from 0 to 30 in steps of 10. The different curves in each panel are related to: (a) v_2' falling in the interval $v_2 \pm 3$, (b) v_2' lower than $v_2 - 3$ (c) v_2' higher than $v_2 + 3$, for the purpose of singling out the vibrational behavior of the colder molecule when the hotter molecule dissociates. In the top lhs panel, where $v_2 = 0$, it is clear that the cross section is completely dominated by case (a). This means that the unexcited molecule essentially remains in its original vibrational state after the dissociative collision. Accordingly, in this case one could adopt a model in which the vibrationally cold ($v_2 = 0$) molecule behaves as a rigid one-body partner. This vibrational adiabaticity cannot be extended to higher v_2 values. In fact, when increasing the value of v_2 it becomes apparent that there is a progressively higher contribution from case (b), implying that the more the colder molecule gets excited, the higher is the contribution of its vibrational energy to the dissociation of the hotter molecule. When the vibrational excitation of the two colliding molecules gets similar, the largest contribution to one-molecule dissociation is due to collisions that leave the undissociated molecule in a quite lower vibrational state. This confirms that, for $v_2 \gg 0$, the vibrational energy of the colder molecule is effective in enhancing dissociation of the hotter molecule, as already highlighted in the comments to fig 2. It is also clear that the vibrational energy of the colder molecule lowers the dynamical threshold of the dissociation of the collisional system. This effect can hardly be modeled in terms of a mere scaling factor of the cross section values, as shown also by other similar results not reported here for brevity.

6. Modeling cold-excited and excited-excited MM collisions

Further indications for the formulation of possible AM/MM scaling are considered in this section by comparing MM(v_1 excited, v_2 excited) CID CSs with MMo(v_1 excited). As evidenced by the comparison shown in the lhs panel of fig 6 between MM CID CSs of molecules with identical vibrational state ($v_1 = v_2$) and the value of the corresponding MMo(v_1), a satisfactory agreement is found only after doubling the value of the latter and scaling its energy of 2/3. The agreement is satisfactory for all the CSs considered, at collision energy 0.5 eV larger than the threshold (less than 0.1 eV for the case of $v = 50$). A rationale for both the scaling factor 2 and the energy displacement of 2/3 can be provided by modeling the generic excited-excited MM(v_1, v_2) CID CS in terms of the sum of the contributions originating from two MM pseudo-cold excited collisions, namely MMo(v_1) and MMo(v_2) ones. The particular case of $v_1 = v_2$ is shown in the left panel of fig 6. The model assumes that the dissociation results from two concurrent events: the collision of molecule 1, considered as pseudo-cold, with molecule 2, considered as excited, and the collision of molecule 2, considered as pseudo-cold, with molecule 1, considered as excited. The basic feature of the model is that in each collision only one atom of the pseudo-cold molecule is assumed to interact with the excited molecule. Moreover, leveraging on the substantial vibrational adiabatic nature of the CID CSs singled out in the previous section when $v_2 = 0$, one is able to estimate the effective collision energy for dissociation. In fact, by taking into account that the relative velocity of the interacting atom of molecule 1 with respect to molecule 2 is on the average the same as in the MM(v_1, v_2) case (only the rovibrational motion can instantly determine a variation), and that in passing from the pseudo AM case to the MM case there is a variation of mass, one can write for the collision energy:

$$E_{\mathrm{MM}} = \frac{\mu_{\mathrm{MM}}}{\mu_{\mathrm{AM}}}\, E_{\mathrm{AM}} = \frac{3}{2}\, E_{\mathrm{AM}} \tag{8}$$

because the collision is considered as an atom-molecule encounter of identical species. As a consequence, for the specific case of $v_2 = v_1$ one obtains:

$$\sigma_{\mathrm{MM}}\left(E_{\mathrm{MM}}, v_1, v_2 = v_1\right) \approx 2\, \sigma_{\mathrm{MMo}}\left(\frac{\mu_{\mathrm{AM}}}{\mu_{\mathrm{MM}}} E_{\mathrm{MMo}}, v_1\right) \tag{9}$$

or more in general:

$$\begin{aligned}\sigma_{\mathrm{MM}}\left(E_{\mathrm{MM}}, v_1, v_2\right) \approx\ & \sigma_{\mathrm{MMo}}\left(\frac{\mu_{\mathrm{AM}}}{\mu_{\mathrm{MM}}} E_{\mathrm{MMo}}, v_1\right) \\ & + \sigma_{\mathrm{MMo}}\left(\frac{\mu_{\mathrm{AM}}}{\mu_{\mathrm{MM}}} E_{\mathrm{MMo}}, v_2\right)\end{aligned} \tag{10}$$

as confirmed by the plots shown in the rhs panel of fig 6, for the case $v_2 = v_1 - 10$.

7. Modeling cold-excited MM collisions from AM corresponding processes

One can now apply the same energy considerations about the energy factor of the preceding section with the aim of finding a simple approximate relationship between AM

CID and cold-excited MMo results. In order to do that, however, further assumptions need to be made in order to take into account the internal energy of the cold molecule. The connection between AM and MMo CID CSs is important, because it allows to approximately reconstruct from AM cross sections the corresponding MMo set, from which in turn one can in principle obtain the other possible combinations of MM excitations by using the approximation presented in the preceding section. Two different procedures are presented here: the first one based on the application of the Levine-Bernstein (LB) model and the second one based on a simple scaling/shifting (SCSH) model.

7.1. Energy-scaled Levine-Bernstein procedure

The LB optical model for atom-molecule dissociation is formulated in ref [75] by considering a 3-body final state analysis in the post-threshold energy region. Under quite general assumptions, the model formulates the AM CID CSs as follows:

$$\sigma_{\mathrm{AM}}(E) = \left(\frac{\pi}{60}\right)\left(\frac{\hbar^2}{2\mu}\right)\left(\frac{2I^*}{\hbar^2}\right)^{5/2}\frac{E'^{5/2}}{E} \tag{11}$$

where E is the AM collision energy, $E' = E + E_{\mathrm{int}} - E_\circ$ (with E_{int} being the molecular internal energy measured from the potential minimum and $E_\circ$ the energy barrier to dissociation), μ is the reduced mass of the AM collisional system and I^* is the moment of inertia of the system about the axis perpendicular to the three-atom plane at a critical configuration. Away from threshold, by dividing the model AM CID CSs of eq 11 by $E'^{5/2}/E$ one obtains a "reduced" cross section that is flat. For illustrative purposes, the reduced cross section obtained by molecular dynamics is plotted in the top panel of fig 7 for different initial vibrational states (v_1 = 20, 30, 40, 50 with lines being AM CID CSs multiplied by the factor 3/2, discussed more in detail later). It is interesting to note that for increasing collision energy all the curves tend to a smooth and flat trend, with quite similar converging values. This is a confirmation of the general validity of the LB model for AM dissociation, at least for the specific systems studied here, with the best results being obtained from low lying vibrational states and high collision energy. A direct and 'ready to use' application of this very smooth trend is shown in Appendix as a result of fitting the calculated AM CID 'rectified' CSs (similar to these reduced CSs), using very few parameters. In the same top panel of fig 7 also the MMo(v) CID reduced CSs are represented in the same manner. Please note that in this case the collision energy is multiplied by 2/3 because of the considerations of the preceding sections applied in this case to real AM collisions in comparison with MMo collisions, and that the energy of the ground vibrational state with respect to the minimum of the diatomic potential is included into E_{int}. Considering that this is a case of cold-excited molecule collision in which only the excited molecule dissociates, while the cold molecule practically does not change its internal state (see the discussion on the vibrational adiabaticity in the preceding section), we adopt for this kind of dissociation the same LB model originally proposed for the AM collisions. The differences between the AM and MMo model

application cases are limited to the introduction of the internal vibrational energy for $v_2 = 0$ in MMo collisions and the different collision energy to consider in the two cases. Concerning I^*, the assumptions made here are the simplest possible: (a) the ratio $I^{*5/2}/\mu$ is approximately constant in passing from N+N_2 to N_2+N_2 collisional system, (b) the (presumably small) collision energy dependence of I^* (which is negligible in the LB model) is practically invariant when substituting N+N_2 with N_2+N_2.

Assumption (a) is scarcely relevant because it introduces at most a constant scaling factor between AM and MMo cross sections, while an inspection of the top panel of fig 7 confirms that assumption (b) is well satisfied. In fact, for each v_1 value, there is a close agreement between AM and MMo curves, when just the threshold region is excluded. As a result, one can reasonably well approximate the cold-excited MMo cross sections as:

$$\sigma_{\mathrm{MMo}}(E) = \mathrm{const}\ \frac{\mu_{\mathrm{MM}}}{\mu_{\mathrm{AM}}} \left(\frac{E'_{\mathrm{MM}}}{E'_{\mathrm{AM}}} \right)^{5/2} \sigma_{\mathrm{AM}}(E) \tag{12}$$

by dividing the AM cross section by its energy dependence and multiplying it by the corresponding MMo energy dependence (in eq 12, $E'_{\mathrm{MM}} = E\ \frac{\mu_{\mathrm{AM}}}{\mu_{\mathrm{MM}}} + E^{\mathrm{int}}_{\mathrm{MM}} - E_\circ$ and $E'_{\mathrm{AM}} = E + E^{\mathrm{int}}_{\mathrm{AM}} - E_\circ$). The $\mu_{\mathrm{MM}}/\mu_{\mathrm{AM}}$ factor in eq.12 comes from using the scaled MM collision energy, as already discussed. This factor is also the origin of the multiplication by 3/2 of AM reduced cross sections in fig 6 (of course, the choice of applying a factor to AM CS instead of MM one is arbitrary). Comparisons of the results of this procedure are shown in the bottom panel of fig 7, where MM CID CSs as a function of collision energy are compared with their approximations obtained from AM CID CSs. The comparisons are quite good for $v = 20$, 30, 40, and acceptable for $v = 50$. It is worth noting that the constant factor of possible discrepancy, cited in connection with the hypothesis (a), is indeed 1 in all the cases studied.

Similar good comparisons can be obtained for results including the $j_1 = 80$ initial rotation of the vibrationally excited molecule, as shown in fig 8. It is important to include also rotation in considering dissociation CSs, due to the very high sensitivity of CID to rotation [47], as well as to the importance now attributed to this dependence in models [37, 45].

However, it is difficult to simulate MMo CID CSs from AM ones when the colder molecule is rotationally excited. For this purpose, in the LB model the internal energy should be inserted in eq 12, but the results are not satisfying. The reasons for this poor performance are likely to be traceable back to the failure of energy scaling under these conditions. In fact, this scaling is justified if the simple model of one "active" atom in the cold molecule of MMo dissociation is valid (see the discussion in the preceding section). Probably, when there is significant rotation in the cold molecule this model is physically unsuited. A better way of introducing the rotational energy of the vibrationally unexcited molecule should be devised. A possibility is to introduce the internal energy of the colder molecule in the LB procedure with a factor less than one. This could be justified because the original model does not concern the colder molecule, that is seen as one body without structure. Empirically one could find this factor as

1/4.

7.2. The scaling/shifting procedure

The second procedure proposed in this paper for the MMo approximation using the AM CID cross sections is based on a simple model where both a scaling of the AM cross section kinetic energy by $\mu_{\rm MM}/\mu_{\rm AM}$ and a shifting of the resulting kinetic energy by the internal energy of the cold molecule are considered:

$$\sigma_{\rm MMo}(E) = \sigma_{\rm AM}\left(E\,\frac{\mu_{\rm MM}}{\mu_{\rm AM}} - E_{\rm int}\right) \tag{13}$$

The scaling is based on the same considerations relative to fig 6 (the MMo CID model involving only one atom of the colder molecule), but in this case the scaling factor is inverted, because the starting point is now (actual, not pseudo) AM kinetic energy to obtain the MMo corresponding quantity. On the other side, the shifting can be rationalized considering that the energy difference between AM and corresponding MMo CID cross sections is due to the presence of a cold molecule in MMo collisions. The application of this very simple model is shown in fig 8, with uniformly quite good results also changing the rotation of the vibrationally excited molecule (j_1 = 0, 40 and 80 in the three panels).

8. Conclusions

Accurate modeling of air plasma chemistry, as in the case of aerothermodynamics or electrical discharges in air, needs elementary processes data with at least the specification of molecular vibration. This is nowadays well recognised in the literature, but the point is that the amount of model input data to treat can be quite large and this is an issue from both the dynamical and kinetic points of view. For this purpose we have developed some relationships between vibrationally dependent atom-diatom and diatom-diatom collision induced dissociation cross sections, based on simple models, and we have illustrated their successful application to the collisions of N+N_2 and N_2+N_2. These relationships can be used to quantitatively obtain diatom-diatom dissociation cross sections from atom-diatom ones, which are much less computationally demanding, with a consequent simplification in the treatment of data also in kinetics. Some 'ready to use' fittings are also provided in the appendix in order to easily obtain diatom-diatom cross sections from atom-diatom data. Even molecular rotation is well treated by the models proposed here, provided it is associated with the vibrationally more excited molecule. The case of rotation in the vibrationally colder molecule is more challenging, and we are actively studying this issue by playing with the internal energy of the colder molecule in the LB model via an efficiency factor less than one.

Obviously difficulties will increase when trying to extend, as we plan to do, similar relationships to more complex collisional systems, especially if they involve different

atomic species, like those including O_2 and NO, in order to enrich the kinetic modeling of earth-air systems.

9. Acknowledgments

We thank the authors of ref [37] for making available their potential energy surface through the POTLIB repository [76]. Thanks are also due to the European Grid Infrastructure (EGI) for supporting the COMPCHEM Virtual Organization and the CMMST Virtual Research Community, the Italian CINECA computing centre under the ISCRA initiative (projects HP10C7RZR8 and HP10CXWOPW) and the OU Supercomputing Center for Education & Research (OSCER) at the University of Oklahoma (OU) for providing computing resources and services. E.G. acknowledges financial support from the MINECO of Spain under grants CTQ2012-37404 and CTQ-2015-65033-P. F.E. acknowledges financial support from Avviso MIUR n. 713/Ric. del 29/10/2010 - Titolo III Creazione di nuovi Distretti e/o Aggregazioni Pubblico Private Intervento di ricerca - PON 03PE_00067_6 "APULIA SPACE".

Appendix

When detailed data are used in kinetic simulations, it is of great importance to have them organized in a way practical to be managed in numerical codes. It is possible to use a functional form suggested by the LB model of ref [75] to formulate a simple fitting function for CID CSs. In fact, provided the LB model is suited to describe the dissociation of the collisional system considered, given the energy dependence in eq 11, it is particularly easy to interpolate almost linear trends resulting from the 'rectified' cross section $(E\sigma(E))^{2/5}$. Related features are shown in the top panel of fig 10 in which AM cross sections from v = 10, 20, 30, 40, 50 are plotted as a function of collision energy, together with the corresponding fitting functions. It is clear from the figure that away from the thresholds the trends are almost linear as expected from the successful application of the model to this collisional system. The resulting parameters of a simple polynomial fit of (at most) third degree, shown in the same figure, are collected in table 1.

The comparison between the AM CID CS computed by molecular dynamics with the curves obtained by inverting $(E\sigma(E))^{2/5}$ using the fitted polynomials are shown in the bottom panel of fig 10. It is worth noting the excellent level of accuracy achieved if one considers the several orders of magnitude spanned by the function and the small number of fitting parameters. With the help of the relationships presented in this paper, one should be able to easily reconstruct from these AM fittings also MM dissociation cross sections with the same atomic species.

Table 1. Parameters of the polynomial fit of the rectified AM cross sections

	a_0	a_1	a_2	a_3
$v = 10$	0.219826	-0.297518	0.038640	0.0
$v = 20$	-2.458287	0.502613	0.000883834	0.0
$v = 30$	-2.296823	0.921919	-0.0260956	0.0
$v = 40$	-1.737670	1.821593	-0.193906	0.00898117
$v = 50^*$	-1.333479	8.684688	-0.414461	0.0168427

* using the square root of the polynomial

[1] Park C 1989 *Nonequilibrium Hypersonic Aerothermodynamics* (New York: Wiley)
[2] Capitelli M, Ferreira C M, Gordiets B F and Osipov A I 2000 *Plasma Kinetics In Atmospheric Gases* Atomic, Optical and Plasma Physics (Heidelberg: Springer-Verlag) ISBN 978-3-540-67416-0
[3] Celiberto R, Armenise I, Cacciatore M, Capitelli M, Esposito F, Gamallo P, Janev R K, Laganà A, Laporta V, Laricchiuta A, Lombardi A, Rutigliano M, Sayós R, Tennyson J and Wadehra J M 2016 *Plasma Sources Sci Technol* **25** 033004
[4] Chikhaoui A, Nagnibeda E, Kustova E and Alexandrova T 2001 *Chem Phys* **263** 111–126
[5] Lino da Silva M, Guerra V and Loureiro J 2009 *Plasma Sources Sci Technol* **18** 034023
[6] Guerra V, Kutasi K, Lino da Silva M, Sa P A and Loureiro J 2010 *High Temp Mater Processes* **14** 141–156
[7] Capitelli M, Celiberto R, Colonna G, D'Ammando G, De Pascale O, Diomede P, Esposito F, Gorse C, Laricchiuta A, Longo S, Pietanza L D and Taccogna F 2011 *Plasma Phys Controlled Fusion* **53** 124007
[8] Capitelli M, Celiberto R, Esposito F, Laricchiuta A, 2009 *Plasma Processes Polym* **6** 279–294
[9] Capitelli M, Armenise I, Bisceglie E, Bruno D, Celiberto R, Colonna G, D'Ammando G, De Pascale O, Esposito F, Gorse C, Laporta V and Laricchiuta A 2012 *Plasma Chem Plasma Process* **32** 427–450
[10] Popov N A 2016 *Plasma Sources Sci Technol* **25** 043002
[11] Capitelli M, Cacciatore M, Celiberto R, De Pascale O, Diomede P, Esposito F, Gicquel A, Gorse C, Hassouni K, Laricchiuta A, Longo S, Pagano D and Rutigliano M 2006 *Nucl Fusion* **46** S260
[12] Armenise I, Esposito F and Capitelli M 2007 *Chem Phys* **336** 83–90
[13] Capitelli M, Armenise I, Bruno D, Cacciatore M, Celiberto R, Colonna G, De Pascale O, Diomede P, Esposito F, Gorse C *et al.* 2007 *Plasma Sources Sci Technol* **16** S30
[14] Belouaggadia N, Armenise I, Capitelli M, Esposito F and Brun R 2010 *J Thermophys Heat Transfer* **24** 684–693
[15] Capitelli M, Colonna G, D'Ammando G, Laporta V and Laricchiuta A 2013 *Phys Plasmas* **20** 101609
[16] Laganà A, Crocchianti S, Aspuru G, Riganelli A and Garcia E 1997 *Plasma Sources Sci Technol* **6** 270–279
[17] Guy A, Bourdon A, Perrin M 2013 *Chem Phys* **420** 15–24
[18] Panesi M, Munafò A, Magin T E and Jaffe R L 2014 *Phys Rev E* **90** 013009
[19] Wysong I, Gimelshein S, Gimelshein N, McKeon W and Esposito F 2012 *Phys Fluids* **24** 042002
[20] Laganà A, Garcia E and Ciccarelli L 1987 *J Phys Chem* **91** 312–314
[21] Garcia E and Laganà A 1997 *J Phys Chem A* **101** 4734–4740
[22] Garcia E, Saracibar A, Gómez-Carrasco S and Laganà A 2008 *Phys Chem Chem Phys* **10** 2552–2558
[23] Wang D, Stallcop J R, Huo W M, Dateo C E, Schwenke D W and Partridge H 2003 *J Chem Phys* **118** 2186–2189
[24] Galvão B R L and Varandas A J C 2009 *J Phys Chem A* **113** 14424–14430
[25] van der Avoird A, Wormer P E S and Jansen A P J 1986 *J Chem Phys* **84** 1629–1635
[26] Stallcop J R and Partridge H 1997 *Chem Phys Lett* **281** 212–220
[27] Cappelletti D, Vecchiocattivi F, Pirani F, Heck E L and Dickinson A S 1998 *Mol Phys* **93** 485–499
[28] Aquilanti V, Bartolomei M, Cappelletti D, Carmona-Novillo E and Pirani F 2002 *J Chem Phys* **117** 615–627
[29] Gomez L, Bussery-Honvault B, Cauchy T, Bartolomei M, Cappelletti D and Pirani F 2007 *Chem Phys Lett* **445** 99 – 107
[30] Hellmann R 2013 *Mol Phys* **111** 387–401
[31] Cappelletti D, Pirani F, Bussery-Honvault B, Gomez L and Bartolomei M 2008 *Phys Chem Chem Phys* **10** 4281–4293
[32] Pacifici L, Verdicchio M, Lago N F L, Lombardi A and Costantini A 2013 *J Comput Chem* **34**

2668–2676
[33] Paukku Y, Yang K R, Varga Z and Truhlar D G 2013 *J Chem Phys* **139** 044309
[34] Paukku Y, Yang K R, Varga Z and Truhlar D G 2014 *J Chem Phys* **140** 019903
[35] Bender J D, Doraiswamy S, Truhlar D G and Candler G V 2014 *J Chem Phys* **140** 054302
[36] Parsons N, Levin D A, van Duin A C T and Zhu T 2014 *J Chem Phys* **141** 234307
[37] Bender J D, Valentini P, Nompelis I, Paukku Y, Varga Z, Truhlar D G, Schwartzentruber T and Candler G V 2015 *J Chem Phys* **143** 054304
[38] Laganà A, Ochoa de Aspuru G and Garcia E 1996 *Quasiclassical and quantum rate coefficients for the N+N_2 reaction* (Perugia (Italy): Centro Stampa Università di Perugia)
[39] Garcia E, Saracibar A, Laganà A, and Skouteris D 2007 *J Phys Chem A* **111** 10362–10368
[40] Rampino S, Skouteris D, Laganà A, Garcia E and Saracibar A 2009 *Phys Chem Chem Phys* **11** 1752–1757
[41] Caridade P J S B, Galvão B R L and Varandas A J C 2010 *J Phys Chem A* **114** 6063–6070
[42] Wang D, Huo W M, Dateo C E, Schwenke D W and Stallcop J R 2004 *J Chem Phys* **120** 6041–6050
[43] Jaffe R, Schwenke D, Chaban G and Huo W 2008 *AIAA* Paper 2008-1208
[44] Jaffe R, Schwenke D and Chaban G 2009 *AIAA* Paper 2009-1569
[45] Panesi M, Jaffe R L, Schwenke D W and Magin T E 2013 *J Chem Phys* **138** 044312
[46] Wang Y, Meng F, Yan P and Wang D 2015 *Chem Phys Lett* **633** 202–207
[47] Esposito F and Capitelli M 1999 *Chem Phys Lett* **302** 49–54
[48] Esposito F, Capitelli M and Gorse C 2000 *Chem Phys* **257** 193–202
[49] Esposito F, Armenise I and Capitelli M 2006 *Chem Phys* **331** 18
[50] Esposito F and Capitelli M 2006 *Chem Phys Lett* **418** 581–585
[51] Li Z, Parsons N and Levin D A 2015 *J Chem Phys* **143** 144501
[52] Cacciatore M, Kurnosov A and Napartovich A 2005 *J Chem Phys* **123** 174315
[53] Kurnosov A, Napartovich A, Shnyrev S and Cacciatore M 2007 *J Phys Chem A* **111** 7057–7065
[54] Kurnosov A K, Napartovich A P, Shnyrev S L and Cacciatore M 2010 *Plasma Sources Sci Technol* **19** 045015 ERRATA CORRIGE: in the paper the term quadrupole-hexadecapole was improperly named quadrupole-octupole.
[55] Kurnosov A, Cacciatore M, Laganà A, Pirani F, Bartolomei M and Garcia E 2014 *J Comput Chem* **35** 722–736
[56] Garcia E, Martínez T and Laganà A 2015 *Chem Phys Lett* **620** 103–108
[57] Bender J D, Nompelis I, Valentini P, Doraiswamy S, Schwartzentruber T, Candler G V, Paukku Y, Yang K R, Varga Z and Truhlar D G 2014 *AIAA* Paper 2014-2964
[58] Bender J D, Valentini P, Nompelis I, Schwartzentruber T E and Candler G V 2015 *AIAA* Paper 2015-3253
[59] Munafò A, Jaffe R L, Schwenke D W, and Panesi M 2015 *AIAA* Paper 2015-0480
[60] Zhu T, Li Z, Parsons N S, Levin D A and Panesi M 2015 *AIAA* Paper 2015-2510
[61] Jaffe R L, Schwenke D W, Grover M, Valentini P, Schwartzentruber T E, Venturi S, and Panesi M 2016 *AIAA* Paper 2016-0503
[62] Kewley D and Hornung H 1974 *Chem Phys Lett* **25** 531–536
[63] Byron S 1966 *J Chem Phys* **44** 1378–1388
[64] Appleton J P, Steinberg M and Liquornik D J 1968 *J Chem Phys* **48** 599–608
[65] Hanson R K and Baganoff D 1972 *AIAA J* **10** 211–215
[66] Lordet F, Méolans J G, Chauvin A and Brun R 1995 *Shock Waves* **4** 299–312
[67] Capitelli M, Armenise I and Gorse C 1997 *J Thermophys Heat Transfer* **11** 570–578
[68] Capitelli M, Celiberto R and Cacciatore M 1994 Needs for cross sections in plasma chemistry *Cross Section Data* (*Advances In Atomic, Molecular, and Optical Physics* vol 33) ed Inokuti M (Academic Press) pp 321–372
[69] The European Grid Infrastructure `http://www.egi.eu`. Last visited 5 July 2016
[70] Laganà A 2005 Towards a grid based universal molecular simulator *Theory of Chemical Reaction Dynamics* (*NATO Science Series II: Mathematics, Physics and Chemistry* vol 145) ed Laganà

A and Lendvay G (Springer Netherlands) pp 363–380
[71] Laganà A, Costantini A, Gervasi O, Faginas-Lago N, Manuali C and Rampino S 2010 *J Grid Comput* **8** 571–586
[72] Rampino S, Monari A, Rossi E, Evangelisti S and Laganà A 2012 *Chem Phys* **398** 192–198
[73] Hase W L, Duchovic R J, Hu X, Komornicki A, Lim K F, Lu D, Peslherbe G H, Swamy K N, van de Linde S R, Varandas A J C, Wang H and Wolf R J 1996 *QCPE Bull* **16** 43
[74] Truhlar D G and Muckerman J T 1979 Reactive scattering cross sections III: Quasiclassical and semiclassical methods *Atom-Molecule Collision Theory* ed Bernstein R B (Springer US) pp 505–566
[75] Levine R and Bernstein R 1971 *Chem Phys Lett* **11** 552–556
[76] Duchovic R J, Volobuev Y L, Lynch G C, Jasper A W, Truhlar D G, Allison T C, Wagner A F, Garrett B C, Espinosa-García J, and Corchado J C, POTLIB, `http://comp.chem.umn.edu/potlib`. Last visited 5 July 2016

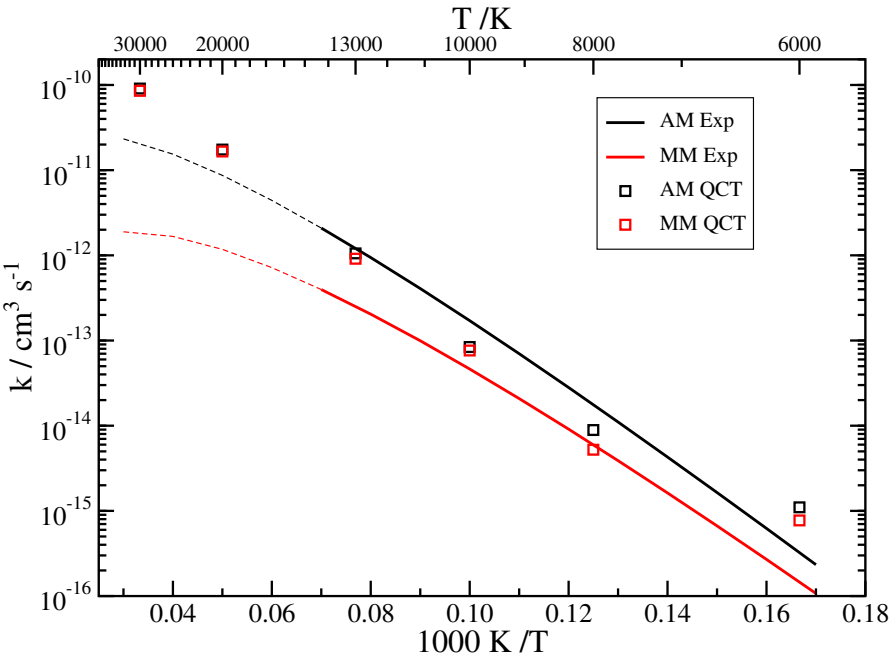

Figure 1. Experimental (lines) and theoretical (squares) thermal Collision Induced Dissociation Rate Coefficients for both the N+N_2 (black) and N_2+N_2 (red) systems. Measured values (continuous lines) falling in the range $T = 6,000 - 14,000$ K are taken from ref [62]. Data extrapolated from the experiment are given as dashed lines up to $T = 30,000$ K.

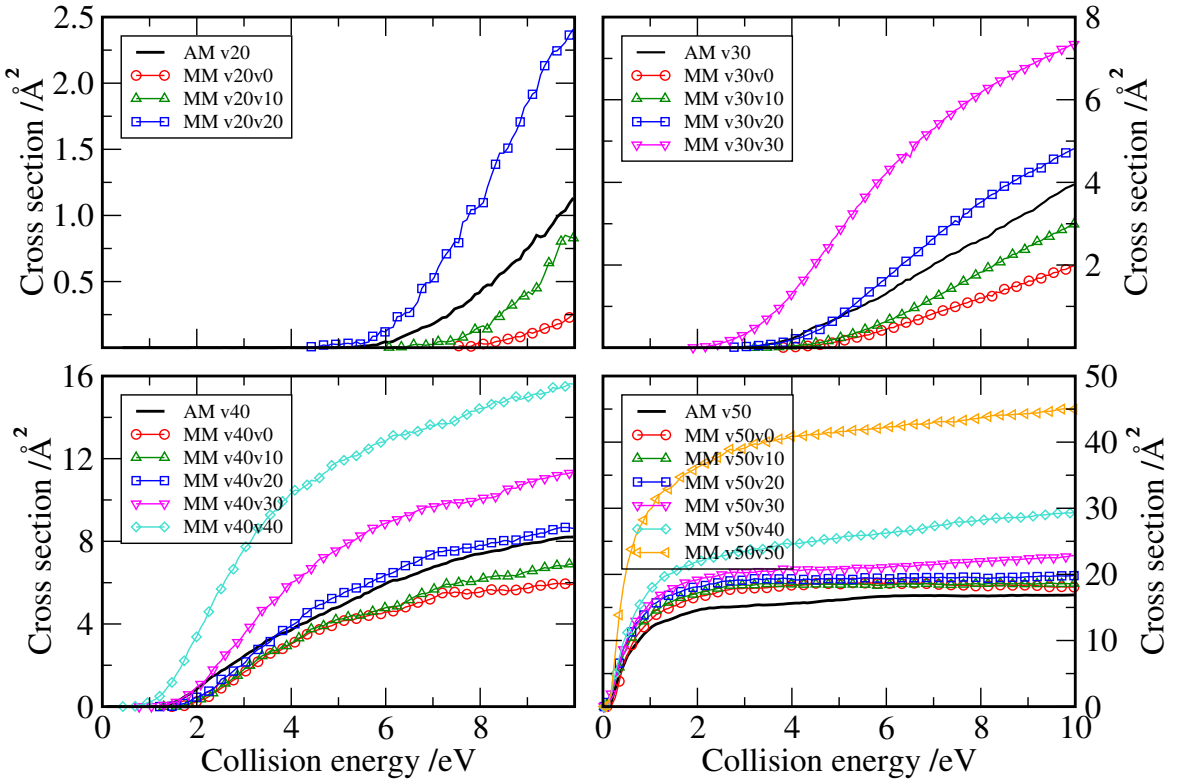

Figure 2. Collision Induced Dissociation Cross Sections computed for the AM system N + $N_2(v_1)$ (solid black line) and for the MM system $N_2(v_2)$ + $N_2(v_1)$ (different symbols and colors are associated with the various values of v_2 that never exceeds v_1) plotted as a function of the collision energy. The value of v_1 increases across the panels from 20 to 50 in steps of 10. The MM colder molecule initial vibrational state v_2 ranges from 0 to v_1 in steps of 10 inside each panel. The initial molecular rotational state is always set equal to zero

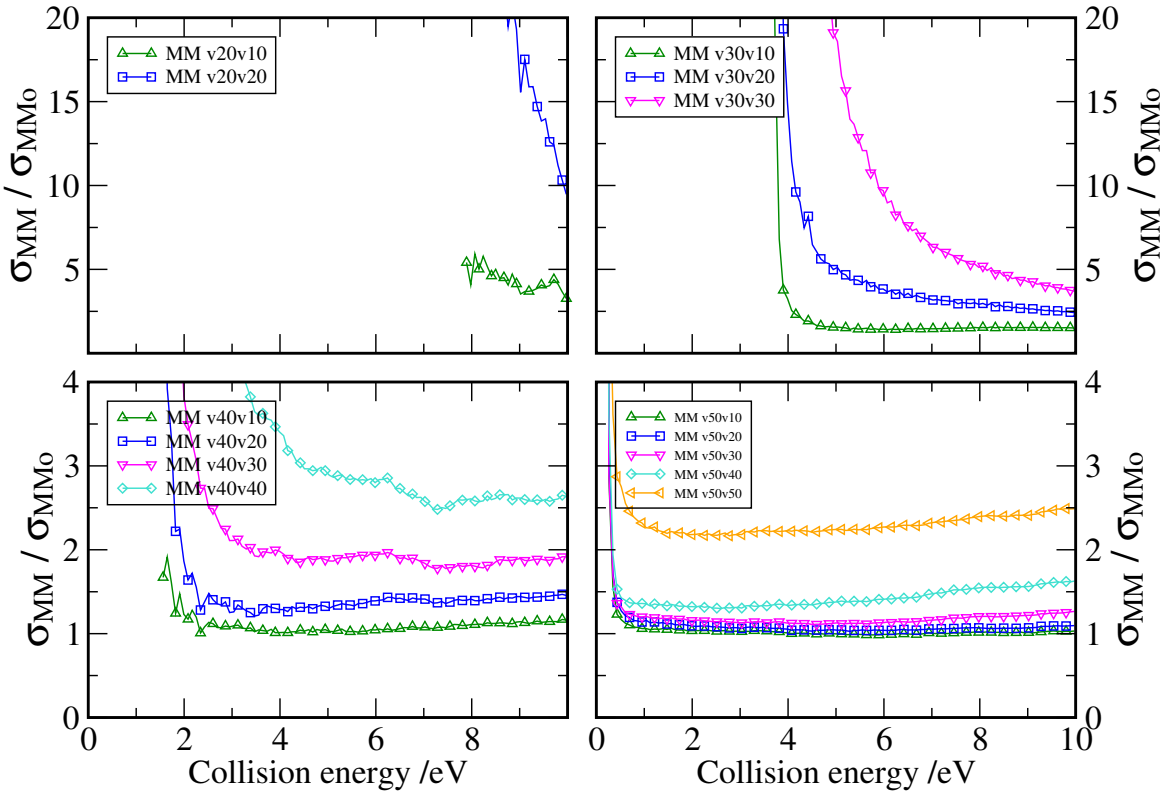

Figure 3. MM(v_1, v_2)/MMo(v_1) Collision Induced Dissociation Cross Section ratio plotted as a function of the collision energy. The value of v_1 increases across the panels from 20 to 50 in steps of 10 and inside each panel the initial vibrational state v_2 ranges from 0 to v_1 in steps of 10. The initial molecular rotational state is always set equal to zero

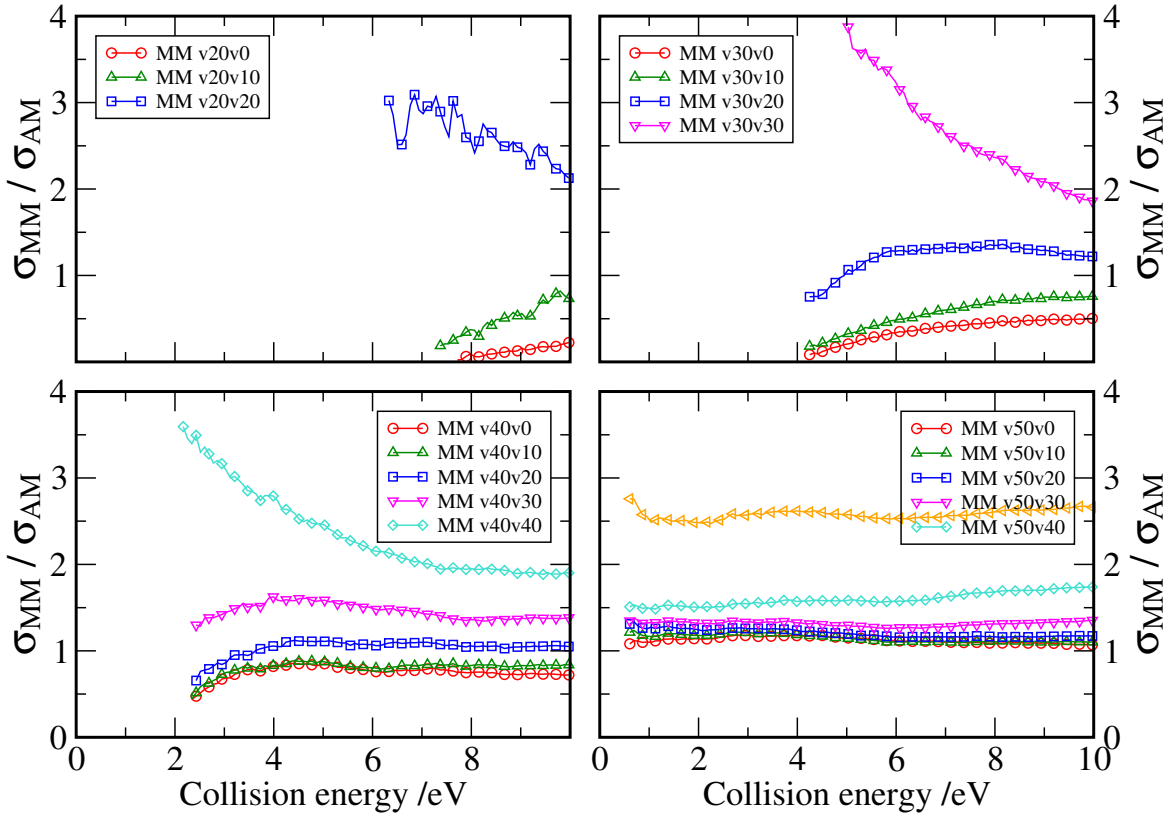

Figure 4. MM(v_1, v_2)/AM(v_1) Collision Induced Dissociation Cross Section ratio plotted as a function of the collision energy. The value of v_1 increases across the panels from 20 to 50 in steps of 10 and inside each panel the initial vibrational state v_2 ranges from 0 to v_1 in steps of 10. The initial molecular rotational state is always set equal to zero

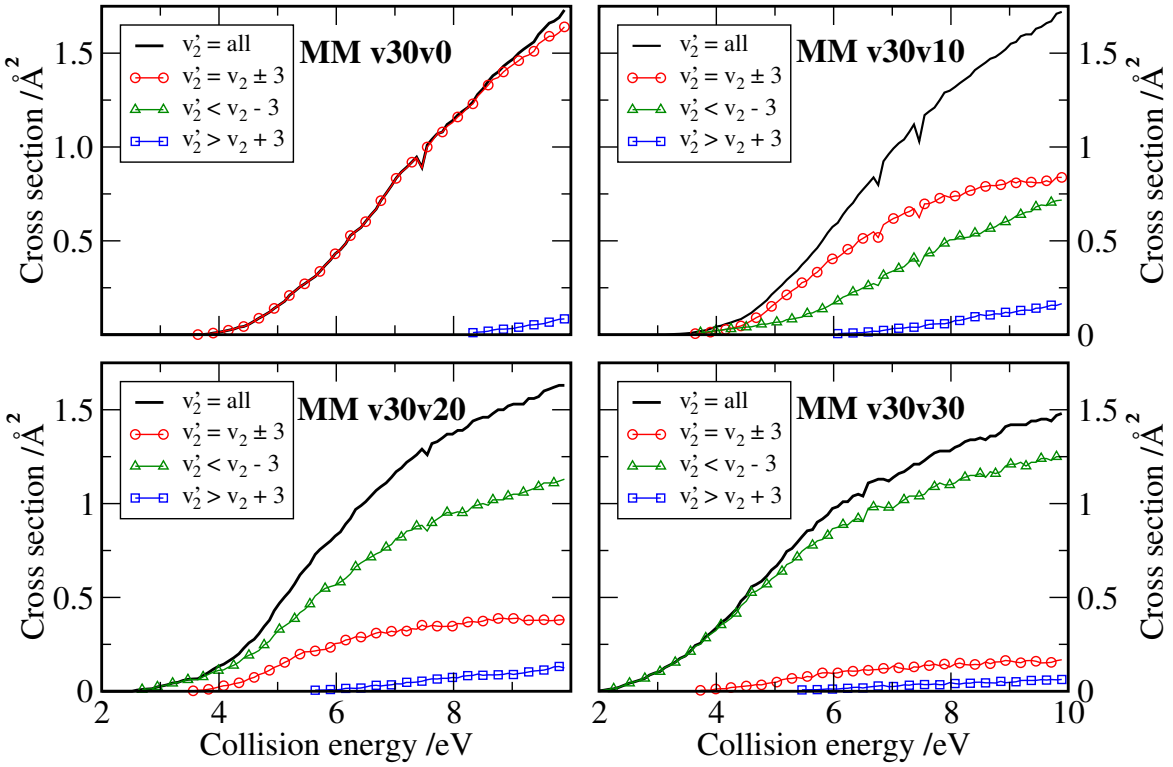

Figure 5. Collision Induced Dissociation Cross Section for the hottest molecule 1 in $N_2(v_1{=}30) + N_2(v_2{=}0{,}10{,}20{,}30)$ collisions, plotted as a function of the collision energy after separating the contributions relative to final vibrational state of the colder non-dissociating molecule into three channels: $v_2' = v_2 \pm 3$, $v_2' < v_2 - 3$, $v_2' > v_2 + 3$.

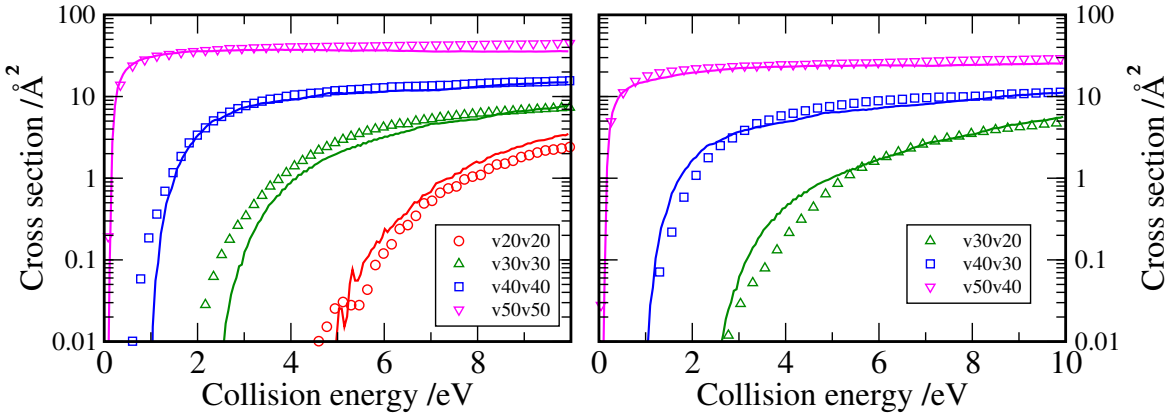

Figure 6. *Left panel*: MM Collision Induced Dissociation Cross Sections from (v_1, v_2), symbols, compared with twice the MMo cross sections from (v_1), lines, plotted as a function of collision energy scaled by a factor 2/3 (see text); *Right panel*: MM Collision Induced Dissociation Cross Sections from (v_1, v_2), symbols, compared with the sum of MMo cross sections from (v_1) and (v_2), lines, plotted as a function of collision energy scaled by the same factor 2/3 (see text).

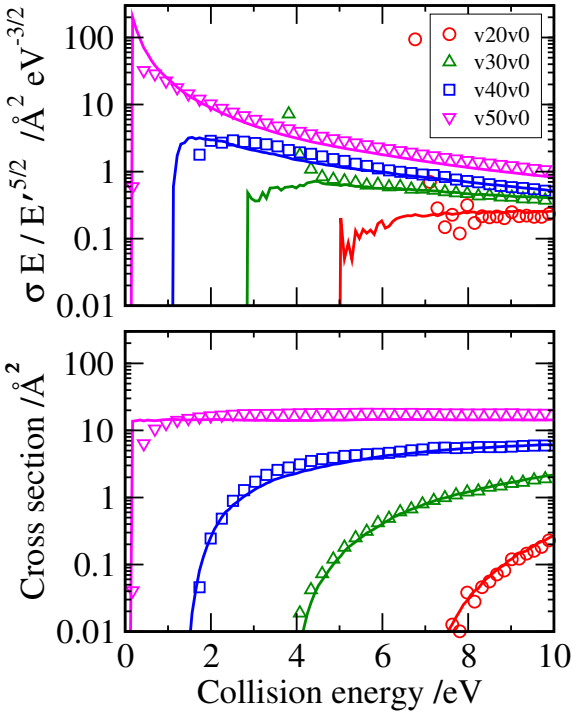

Figure 7. *Top panel*: MMo(v_1), symbols, and AM(v_1), lines, Collision Induced Dissociation Cross Sections divided by the energy dependence in the Levine-Bernstein model, plotted as a function of collision energy. *Bottom panel*: Comparison of computed MMo(v_1), symbols, Collision Induced Dissociation Cross Sections with corresponding values derived from AM(v_1) cross sections using the energy-scaled Levine-Bernstein procedure, lines, plotted as a function of collision energy.

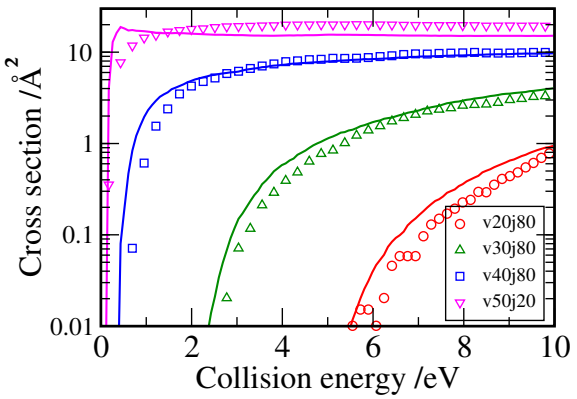

Figure 8. Comparison of computed MMo(v_1,j_1=80), symbols, Collision Induced Dissociation Cross Section with corresponding values derived from AM(v_1,j_1=80) ones, lines, using the energy-scaled Levine-Bernstein procedure, plotted as a function of collision energy.

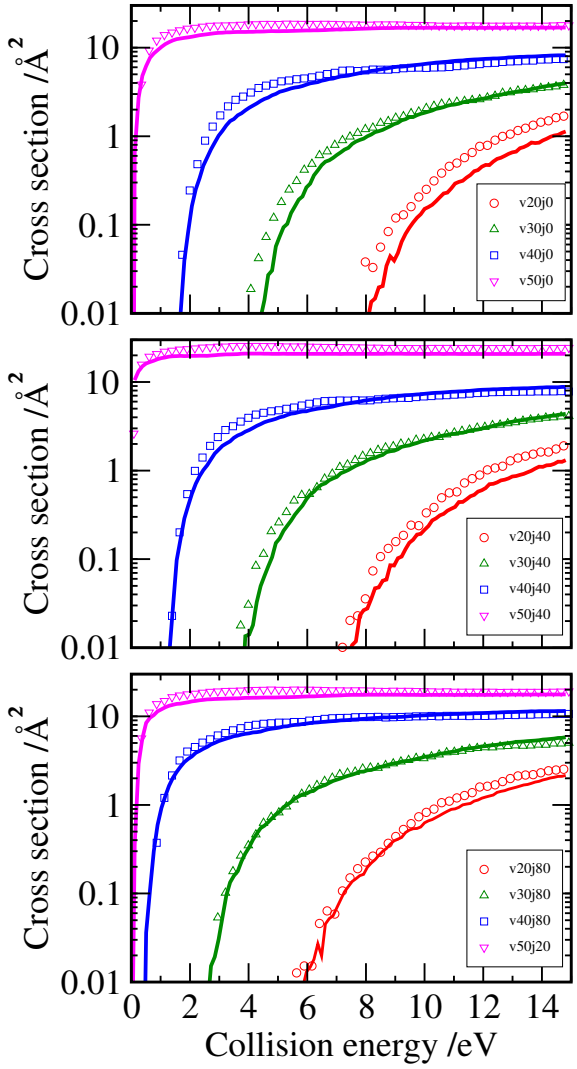

Figure 9. Comparison of computed MMo(v_1,j_1=0,40,80), symbols, Collision Induced Dissociation Cross Section with corresponding values derived from the AM(v_1,j_1=0,40,80) ones, lines, using the scaling/shifting model, plotted as a function of collision energy.

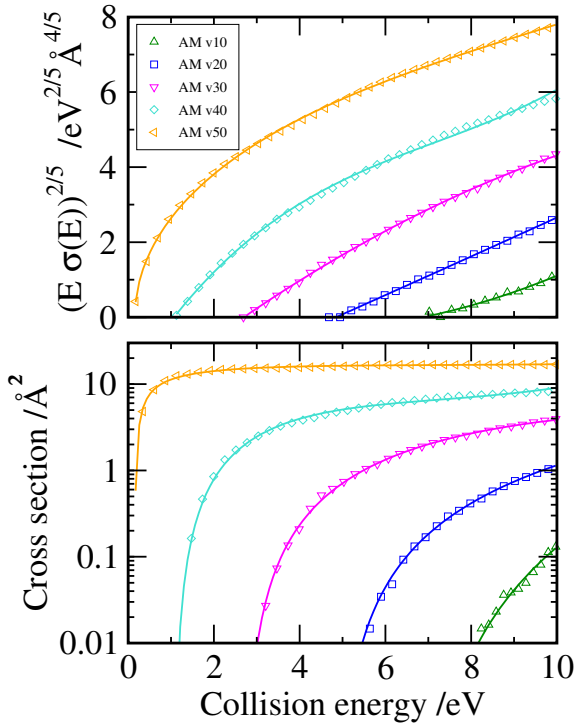

Figure 10. *Top panel*: Interpolation, lines, of AM(v_1), symbols, "rectified" Collision Induced Dissociation Cross Sections using a third degree polynomial (see text), plotted as a function of collision energy. *Bottom panel*: AM(v_1), symbols, Collision Induced Dissociation Cross Sections and the resulting interpolation lines, plotted as a function of collision energy.